INDIAN JOURNAL OF SCIENCE AND TECHNOLOGY

RESEARCH ARTICLE

Study of Structural, Morphological, Electrical, and Thermal Characteristics of PPy-Fe(ClO_4)$_2$ -Au Nanocomposite and its Application in Ammonia Gas Sensing

Vinod S More[1]*, Minal P Patil[1], Raju P Tandel[2], Tatyarao N Ghorude[1], Gitesh G Padhye[3]

1 G.E.S.s, N. B. Mehta Science College, Bordi, Dahanu, Palghar, Maharashtra, India
2 SDSM Dandekar College, Palghar, Maharashtra, India
3 Thakur College of Science and Commerce, Kandivali (East), Mumbai, India

OPEN ACCESS

Received: 30-09-2024
Accepted: 29-11-2024
Published: 18-12-2024

Citation: More VS, Patil MP, Tandel RP, Ghorude TN, Padhye GG (2024) Study of Structural, Morphological, Electrical, and Thermal Characteristics of PPy-Fe(ClO_4)$_2$ -Au Nanocomposite and its Application in Ammonia Gas Sensing. Indian Journal of Science and Technology 17(46): 4842-4853. https://doi.org/10.17485/IJST/v17i46.3148

* **Corresponding author**.

vinod13570@gmail.com

Funding: None

Competing Interests: None

Published By Indian Society for Education and Environment (iSee)

ISSN
Print: 0974-6846
Electronic: 0974-5645

Abstract

Objectives: The synthesis of Polypyrrole based nanocomposites using chemical techniques and then characterize using various techniques to study the Structural, morphological, and Thermal characteristics of these materials. The main objective of this research is to fabricate room temperature operative NH_3 gas sensor. **Methods:** Turkevich method is used for the synthesis of gold nanoparticles. These Gold nanoparticles are further employed to form polypyrrole-based nanomaterials using the Chemical oxidative polymerization method. These nanocomposites were comprehensively characterized using SEM, TEM, X-ray Diffraction, FTIR, UV-vis Spectroscopy, and TGA. The two-probe approach was used to measure electrical conductivity. Synthesized PPy-Fe(ClO_4)$_2$-Au nanocomposite was then applied to fabricate room temperature operated gas sensor that can detect ammonia (NH_3) gas at low ppm levels. **Findings:** The SEM of the PPy based nanoparticle shows its globular morphology with size in 180-250 nm. XRD shows an amorphous nature with some crystalline formation indicating Au presence. FTIR reveals prominent peaks showing significant bonds of PPy. The UV-visible spectra of pure PPy shows a peak at 349 nm while PPy-Fe(ClO_4)$_2$ and PPy-Fe(ClO_4)$_2$-Au show additional peak at 541 nm and 421 nm. The I-V characteristic of PPy-Fe(ClO_4)$_2$-Au shows enhanced conductivity of 30.58 Scm^{-1} which is higher than pure PPy. **Novelty:** A novel dopant Iron(II) per chlorate Fe(ClO_4)$_2$, was added to the nanoparticles to synthesize PPy-Fe(ClO_4)$_2$-Au nanocomposites. Since most of the sensors worked at some elevated temperature, this paper presents low ppm level NH_3 gas sensing at room temperature which is the key step for this research work.

Keywords: PPy; AuNPs; Polypyrrole; NH_3; PPy-AuNPs-Fe(ClO_4)$_2$

1 Introduction

In recent times, gas sensors have been developed with growing demand and utilized in various sectors such as environmental monitoring, the automotive industry, medical applications, and indoor air quality management. Ammonia (NH_3) is a hazardous gas that has attracted considerable interest in gas detection research due to its extensive production and consumption worldwide[1]. The majority of ammonia exposure occurs in agriculture due to the use of powerful fertilizers, although it is also widespread in mining, metallurgy, petroleum refining, specialty workers handling commercial refrigerants or de-icing, and agricultural workers handling significant amounts of fertilizer[2]. Short-term exposure to ammonia can result in burns to the skin and eyes, while even low concentrations can irritate the respiratory system, nose, and throat and induce freeze burns. The worst risk occurs when ammonia reacts with body fluids to create ammonium hydroxide, which can cause instant internal burns, tissue death, and even blindness. This highlights the vital necessity of gas sensors in sectors with significant ammonia exposure[1,2]. Advances in nanotechnology attracted researchers to fabricate gas sensors based on conducting polymers which can sense gases at room temperature with high sensitivity[3].

Conducting polymers (CPs) are an emerging class of beneficial compounds. They have sparked great interest in a variety of disciplines due to their simplicity of production, anti-corrosion properties, light-weight nature, cost-effectiveness and exceptional electrical, mechanical, and optical characteristics[4]. Among many conducting polymers such as Polyacetylene, polyaniline and polypyrrole, the most promising conducting polymer according to many researchers is Polypyrrole (PPy). PPy has superior environmental stability, simple synthesis, along with its excellent conductivity[5].

There are numerous methods for synthesizing PPy, including Chemical, vapor phase deposition and electrochemical processes. Chemical oxidation is a simple, fast, affordable, and reliable method among them. In this paper, the synthesis of PPy nanocomposites with gold nanoparticles is presented. Iron(III) Chloride ($FeCl_3$) is used as an oxidant and iron perchlorate ($Fe(ClO_4)_2$ is utilized as dopant. Initially, pyrrole monomers react with $FeCl_3$ to create PPy, which is followed by the byproducts $FeCl_2$ and HCl. The next step involves doping PPy with $Fe(ClO_4)_2$, the process followed according to the literature[6,7]. This allows the perchlorate ions (ClO_4^-) to be incorporated into the polymer chain, stabilizing the positive charges and enhancing electrical conductivity. The total reaction yields doped polypyrrole with the perchlorate ions acting as dopants to enhance the conducting characteristics of the polymer.

When dopant Fe $(ClO_4)_2$ is added to PPy, it produces ClO_4^- anions, which are critical in the doping process. Positive charges such as polarons and bipolarons are introduced into the PPy structure by doping with ClO_4^- ions. This facilitates a charge-transfer mechanism that substantially enhances the conductivity of the polymer. This dopant balances the positive charges on the PPy structure, stabilizing the polymer's conductive state and increasing electrical conductivity. Improved charge mobility is a result of the additional electron delocalization made possible by the presence of Fe^{2+} ions from Fe $(ClO_4)_2$. A nanocomposite with improved conductivity, thermal stability, and appropriateness for gas sensing applications is produced as a result of this charge stabilization, which also improves the PPy structure's overall electrical characteristics.

In order to improve PPy's electrical characteristics, the majority of studies have concentrated on adding conventional dopants like organic chemicals, transition metal salts, and metallic nanoparticles. Studies have demonstrated that by encouraging interactions between the polymer and target gas molecules, doping with metals like gold, silver, and copper or organic compounds like camphor sulfonic acid enhances gas sensing sensitivity. There is currently a significant gap that has to be filled and an opportunity for innovation because dopant $Fe(ClO_4)_2$ used in our study has not been documented in recent literature. These samples were characterized by SEM (Scanning Electron Microscope), TEM (Transmission Electron Microscope), XRD (X-ray Diffraction), FTIR (Fourier Transform Infrared) Spectroscopy, UV-visible spectroscopy and TGA (Thermogravimetric Analysis). These were then utilized to determine electrical conductivity using two probe method[8]. Finally, the sample with higher conductivity was used to study gas sensing characteristics for detecting NH_3 gas.

Sood et al. synthesized polypyrrole (PPy) using ammonium peroxydisulfate (APS) and ferric chloride ($FeCl_3$), finding that $FeCl_3$-based PPy exhibited higher conductivity ($2.22 \times 10^-$ S/cm) and better thermal stability than APS-based PPy[9]. Pagar et al. used a chemical approach to manufacture PPy, which was then analyzed using SEM, XRD, FTIR, and UV-visible spectroscopy at various Molar ratios[10]. Dave et al. produced PPy by employing ferric chloride as an oxidant with different oxidant-to-monomer ratios with the conductivity of the samples ranging from 545.19 μScm^{-1} to 215.78 μScm^{-1}[11]. Sravanthi et al. used a variety of sulphonic and inorganic acid dopants along with ammonium persulfate as an oxidant to create PPy using chemical oxidative polymerization, this suggests that PPy produced in sulphonic acid media had greater conductivity[12].

The aim of this study is to synthesize PPy, PPy doped with $Fe(ClO_4)_2$ and PPy-$Fe(ClO_4)_2$-Au nanocomposite for oxidant to monomer molar ratio (M.R.) 1:1 and characterize with various techniques. Synthesized nanocomposite samples were investigated for electrical conductivity measurement and finally PPy-$Fe(ClO_4)_2$-Au nanocomposite was utilized for NH_3 gas sensing study.

2 Methodology

2.1 Materials

The monomer Pyrrole (AR grade) was purchased from Spetrochem Pvt. Ltd., Mumbai, and stored in a dark bottle at a low temperature. Iron(III) chloride ($FeCl_3.6H_2O$) of 97% AR grade was procured from Loba Chemie. Chloroauric Acid ($HAuCl_4$), trisodium citrate and Iron(II) perchlorate ($Fe(ClO_4)_2$) were obtained from Molychem. Synthesis of nanocomposites was done under the double distilled water.

2.2 Methods

2.2.1 Synthesis of PPy:

Polypyrrole (PPy) was synthesized using a chemical oxidative technique[9,13]. $FeCl_3$ acted as the oxidant and pyrrole as the monomer. Double distilled water was used to prepare a 1 M pyrrole solution, which was then pre-cooled in an ice bath (0–5°C) while being continuously stirred slowly for 30 minutes with a magnetic stirrer. Then, while keeping the ice bath conditions for three to four hours, a precooled 10 ml of $FeCl_3$ solution was poured in dropwise with a monomer to oxidant molar ratio (M.R.) of 1:1. To ensure complete polymerization, the mixture was then allowed to settle for an entire day. To get rid of any unreacted monomer, oxidant, and ferrous or ferric contamination, the resultant precipitate was filtered under reduced pressure and then washed with distilled water. The product was then vacuum-dried at room temperature until it reached a consistent weight[13]. The same process was used to prepare a second sample, which was doped with 0.1 M $Fe(ClO_4)_2$ for three hours while being stirred at a low temperature and constant speed. The final Monomer:Oxidant:Dopant molar ratio is 1:1:0.1 which is found to be good for getting high yield. The resulting powder was then cleaned and filtered to provide PPy doped with $Fe(ClO_4)_2$.

2.2.2 Synthesis of Gold Nanoparticles (AuNPs):

Turkevich method was used to create citrate-stabilized gold nanoparticles[14]. A standard experiment involved heating 100 ml of 0.5 mM $HAuCl_4$ to boiling. This solution was treated with 10 ml of 38 mM trisodium citrate, which started the reduction of $HAuCl_4$. Successful AuNP production was indicated by the solution changing from translucent yellow to violet and then to ruby red after 8 to 9 minutes of vigorous mixing. Trisodium citrate worked as a reducing as well as stabilizing agent[14].

2.2.3 Synthesis of Polypyrrole iron(II) perchlorate Gold (PPy-Fe(ClO_4)$_2$-Au) nanocomposite:

The PPy-$Fe(ClO_4)_2$-Au nanocomposite was created by in situ chemical oxidative polymerization. First, a magnetic stirrer was used to agitate 40 ml of a 0.5 mM AuNP colloidal solution for ten minutes while it cooled in an ice bath. The gold nanocomposite was then formed by adding 1 M pyrrole solution, and the mixture was stirred for 30 minutes to produce a homogeneous solution. The reaction mixture was then kept at 0–5°C for an hour while magnetic stirring was maintained. A precooled 1 M ferric chloride solution was subsequently added by drops over 30 minutes with monomer to oxidant ratio of 1:1. Then, for three hours, a 0.1 M $Fe(ClO_4)_2$ dopant was added while being constantly stirred in an ice bath. The polymerization process was then completed by allowing the solution to be settled overnight. The product was filtered under reduced pressure, washed with distilled water until the filtrate was colorless, and vacuum-dried at room temperature.

We regulated the PPy solution's pH between 1-3, since the highest precipitation is achieved at an acidic (lower) pH of about 1.1 and the least amount at higher pH values, such as 5. A calibrated pH meter was used to test the pyrrole solution's initial pH, and diluted acid was added in order to adjust it. The oxidative polymerization of pyrrole monomers is favored by acidic conditions, which guarantee a constant reaction rate and improve conductivity through efficient doping. $FeCl_3$ functions as an effective oxidant at these lower pH values, promoting stable and consistent PPy production. Similar pH monitoring was done for the AuNP solution to ensure steady nanoparticle production, and modifications were implemented to sustain desired conditions.

2.2.4 Characterization and Conductivity Measurement:

All the samples were characterized by utilizing a wide range of modern techniques to ensure a comprehensive understanding of their characteristics. Utilizing the FEI Quanta 200 model, we performed SEM for the identification of surface morphology. The FEI Tecnai G2-F30 was used to conduct Transmission Electron Microscopy (TEM) studies to investigate the interior nanostructure. To find out the crystalline structure, an XRD analysis was conducted using the PANalytical Empyrean, Malvern. In order to study chemical bonding and molecular composition, Fourier Transform Infrared (FTIR) spectra were obtained using Bruker, Germany's Attenuated Total Reflectance technology (ATR). Agilent Technologies Cary 100 UV-vis spectroscopy was used to examine the optical characteristics. To validate thermal stability and composition, TGA was performed using Hitachi

NEXTA STA300. The final product was pressed into pellets, and their electrical conductivity was measured using the two-probe method. Ultimately, these extensively studied and electrically verified samples were utilized to fabricate gas sensors, applying their improved characteristics to enhance sensing performance.

2.2.5 Gas Sensing Setup and Interdigitated Electrode (IDE):

CPs deposited on IDE were used to monitor the gas response in a specially built gas chamber with a volume of 1000 cm^3. The schematic representation of the gas sensing unit used in the research is shown in Figure 1. The gas concentration inside the chamber can be accurately regulated by injecting an accurately measured quantity of gas from a calibrated source with a syringe, which is connected to a pressure gauge for monitoring and controlling ppm levels. For the purpose of testing and analyzing sensors, this technique provides precise gas concentration modification to the required levels. The resistance of the conducting Polypyrrole (PPy) layer deposited on the IDE sensor was measured using a Keithley 2000 digital multimeter. To quantify sensor recovery, air was forced into the chamber until equilibrium was attained. This was accomplished by opening valves V1 and V_2 at the same time while running a vacuum pump. While valve V_1 permitted the entry of new air, accelerated by the vacuum pump, valve V_2 enabled the release of gas. All the sensitivity tests were conducted at room temperature.

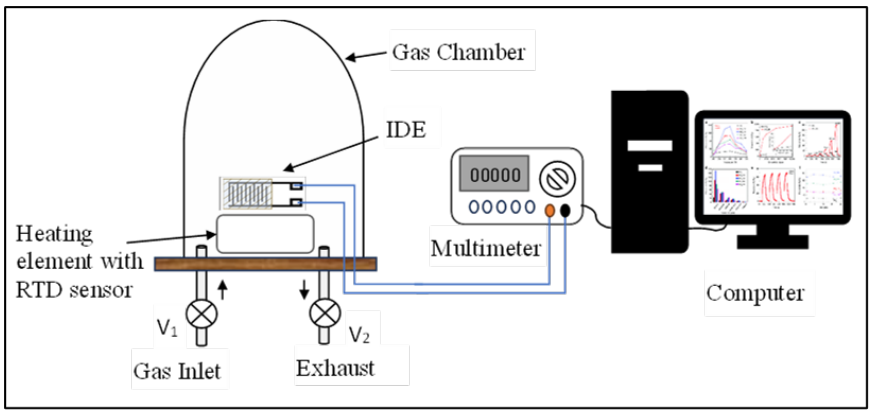

Fig 1. Schematic of Gas Sensing Setup

The interdigitated electrodes in the IDE sensor were formed by screen-printed copper tracks with a spacing and width of about 1 mm, which were placed onto an epoxy glass basis. The overall dimensions of the sensor device were 30 mm by 20 mm. For the production of the sensor, PPy powder was mixed with polyvinyl alcohol, stirred, and subsequently brush-coated onto IDE substrates. These sensors which are critical for measuring gas sensing capabilities, vacuum dried before testing.

3 Result and Discussion

Several characterizations were performed on Pure PPy, PPy doped and PPy-$Fe(ClO_4)_2$-Au nanocomposites as follows:

3.1 SEM and TEM analysis:

The SEM of Pure PPy, PPy-$Fe(ClO_4)_2$ and PPy-$Fe(ClO_4)_2$-Au nanocomposite is illustrated in Figure 2. All of these are generally showing globular morphology consistent with structures reported by Sood et.al.[9]. The Figure 2**a** shows the closely packed structure with inter-junction formations while the Figure 2**b** shows that the particles of dopant were largely distributed on the PPy matrix. $Fe(ClO_4)_2$ contributes electron-withdrawing properties which increase the charge density in the PPy matrix. This improves the arrangement of polymer chains and generates more conduction sites, thereby enhancing the conductivity of the polymer. Furthermore, the addition of the dopant increases the material's interaction with the targeted gas molecules. Figure 2**c** demonstrates that the PPy-$Fe(ClO_4)_2$-Au nanocomposite has a densely packed structure with uniform distribution, resulting in a large number of inter-junction forms on the surface of the synthesized material. When the target gas is exposed, these junctions allow a large number of majority charge carriers to pass across the composite, thus improving the gas sensing performance[15]. The addition of Au nanoparticles and dopant increases the number of adsorption sites in the composite material, indicating that it may perform better in gas-sensitive applications than pure PPy[16]. The size of these particles is in the range of 180-250 nm. Figure 2 **d** shows the High-resolution TEM of PPy-$Fe(ClO_4)_2$-Au nanocomposite. The bright

areas illustrate the Scherrer ring pattern, which represents the fcc gold crystalline structure[17]. The circular structure confirms the presence of gold nanoparticles which were attached to the PPy matrix. The size of the Au particle is in the nanometer range (~40 nm)[18].

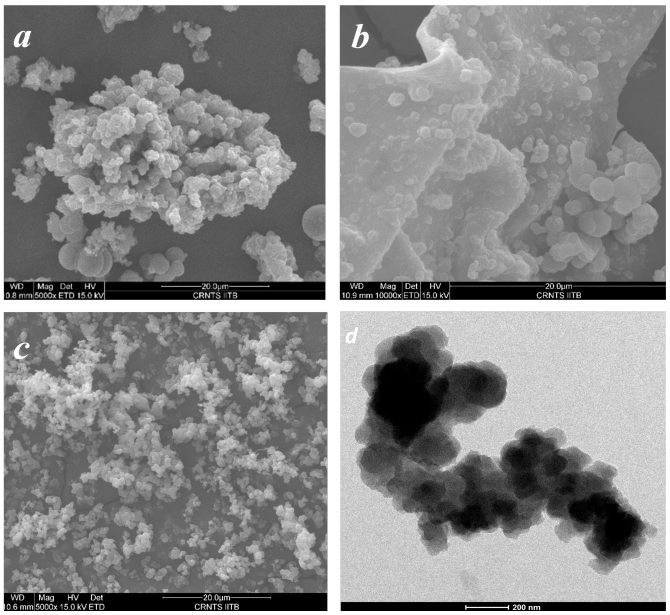

Fig 2. SEM micrographs of the nanocomposites: a) Pure PPy, b) PPy-Fe(ClO_4)$_2$ c) PPy-Fe(ClO_4)$_2$-Au nanocomposite and d) TEM of PPy-Fe(ClO_4)$_2$-Au nanocomposite

3.2 XRD analysis:

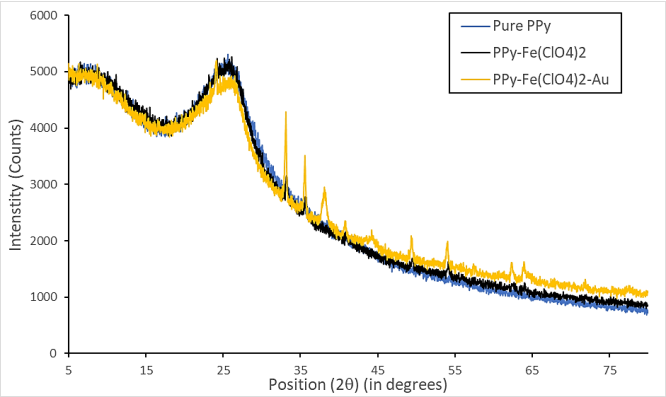

Fig 3. XRD of Pure PPy, PPy-Fe(ClO_4)$_2$ and PPy-Fe(ClO_4)$_2$-Au nanocomposite

Figure 3 describes the XRD spectra of Pure PPy, PPy-Fe(ClO_4)$_2$ and PPy-Fe(ClO_4)$_2$-Au nanocomposite. All of these spectra indicate that all are amorphous in nature except PPy-Fe(ClO_4)$_2$-Au nanocomposite which has some additional sharp peaks. The XRD sample of all these samples shows a broad hump around 20-30º which confirms the existence of PPy consistent with the results recorded in previous literature[19,20]. When dopants are added, the π-bonds overlap more, bringing the polymer chains closer together and enhancing electrical conductivity. Fe(ClO_4)$_2$ introduces perchlorate (ClO_4^-) ions that interact with the positively charged structure of doped PPy. These interactions may allow for more regular alignment of the polymer chains, enhancing crystalline regions. However, the XRD of PPy-Fe(ClO_4)$_2$-Au hybrid nanocomposite shows some sharp peaks at some 2θ values such as 26.65, 33.14, 35.60 and 38.09 which confirms the presence of Au nanoparticles[14,18]. Using the Scherrer

equation (shown below), the average crystallite size of PPy-Fe$(ClO_4)_2$-Au nanocomposite was calculated as ~40 nm which is consistent with the size of the Au nanoparticles shown in TEM results.

Scherrer equation [21] is given by,

$$D = \frac{k\lambda}{\beta cos\theta}$$

where D stands for crystalline size, K for Scherrer constant, λ for wavelength of the applied X-ray beam (1.54184 Å), β for peak Full width at half maximum (FWHM) and θ for Bragg angle.

Table 1. Crystallite size as per each peak using Scherrer equation

Peak (2θ)	Crystallite sizes (nm)
24.12	41.63
40.83	57.93
49.41	44.81
54.08	45.71
62.36	47.59

3.3 FTIR analysis:

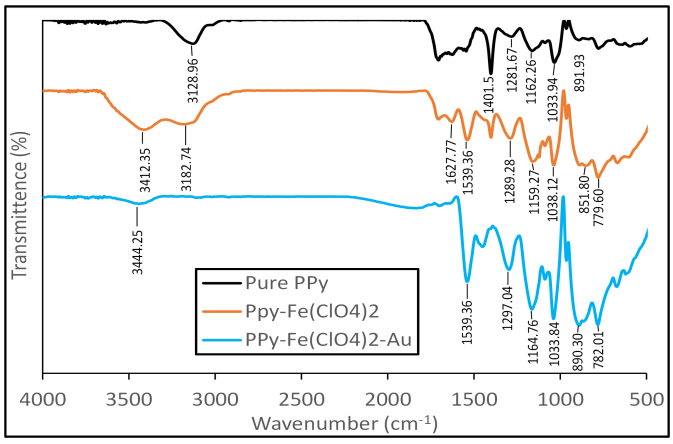

Fig 4. Infrared spectra of Pure PPy, PPy-Fe$(ClO_4)_2$ and PPy-Fe$(ClO_4)_2$-Au nanocomposite

The IR spectra of Pure PPy, PPy-Fe$(ClO_4)_2$ and PPy-Fe$(ClO_4)_2$-Au hybrid nanocomposite recorded from 4000 to 500 cm^{-1} is illustrated in Figure 4. Each of the IR curves has a band at 3128.96, 3418.25, and 3444.25 cm^{-1}, which is associated with the N–H stretch vibration [13]. The pyrrole ring vibration is responsible for the major band at 1627.77 and 1539 cm^{-1} [9]. The spectra of PPy-Fe$(ClO_4)_2$ and PPy-Fe$(ClO_4)_2$-Au show small variations in peak locations compared to pure PPy. This suggests interactions between the dopant (Fe$(ClO_4)_2$, Au nanoparticles, and the PPy matrix. Fe^{2+} ions and ClO_4^- anions interact electrostatically with the PPy backbone, stabilizing its charged structure and shifting vibrational modes. The =C–H in-plane vibration is correlated with the band at 1033.94, 1038.12 and 1038.84 cm^{-1} [10]. The N=C stretching vibration is responsible for the band at 1281.67, 1289.28 and 1297.04 cm^{-1} [11]. The peaks at 1162.26, 1159.27 and 1164.76 are due to the C-H in plane bending [10].

Furthermore, Au nanoparticles interact with PPy's nitrogen sites via charge transfer, contributing to these modifications. These coupled interactions cause structural alterations and restructuring of the PPy chain conformation, altering vibrational energy and producing the observed FTIR peak shifts. The bipolaron structure of PPy is distinguished by unique vibrations in the C=N, C=C, and N-H regions. When compared to the distinctive FTIR peaks of pure PPy, the PPy-Fe$(ClO_4)_2$-Au nanocomposite's spectrum clearly shows certain modifications, which indicate the inclusion of gold into the polymer matrix. According to spectroscopic characterization of polypyrrole, all the peaks show absorption peaks corresponding to bipolaron

bands, which were observed at 891.93, 851.80, and 890.30 cm^{-1} [5]. Since bipolaron generation raises the density of charge carriers, it improves conductivity. Bipolarons have the ability to interact with gas molecules in gas sensing, which can alter the sensor's electrical characteristics. The peaks present in FTIR of all samples were consistent with Pagar et.al. [10], Dave et.al. [11], Sood et.al. [9] and Kadhem et.al. [5].

3.4 UV-visible spectroscopy:

During the formation of gold nanoparticle, the gold colloidal solution made of $HAuCl_4$ first turns into colourless then Pink, and at last it becomes Ruby red which is required. The UV-visible spectra of gold nanoparticle solutions are shown in Figure 5 **a, b** and **c** respectively. The characteristics peak for all these graphs is about 527, 531 and 528 nm which confirms the existence of gold nanoparticle [14]. One important physical characteristic of AuNPs is surface plasmon resonance (SPR). As the core size increases from 1 to 100 nm, spherical AuNPs in aqueous solution display a range of colors and they frequently show a size-relative maximum absorption within 500 and 550 nm [22]. When gold nanoparticles were forming, the absorption spectrum showed a SPR peak at 530 nm; the red-shift with growing particle size showed that the development of gold nanoparticles was successful [23].

Figure 5**d** shows UV-vis spectra of the Pure PPy, PPy-Fe$(ClO_4)_2$ and PPy-Fe$(ClO_4)_2$-Au nanocomposite. Polypyrrole's characteristic bands show π-π^* transitions for C=C at around 270 nm. The pure PPy shows a peak at 349 nm [24] while PPy-Fe$(ClO_4)_2$ and PPy-Fe$(ClO_4)_2$-Au show additional peak at 541 nm and 421 nm can which suggests the presence of dopant. The peak observed at 527 nm and 561 nm indicates the formation of gold nanoparticles according to the Borse et.al [17].

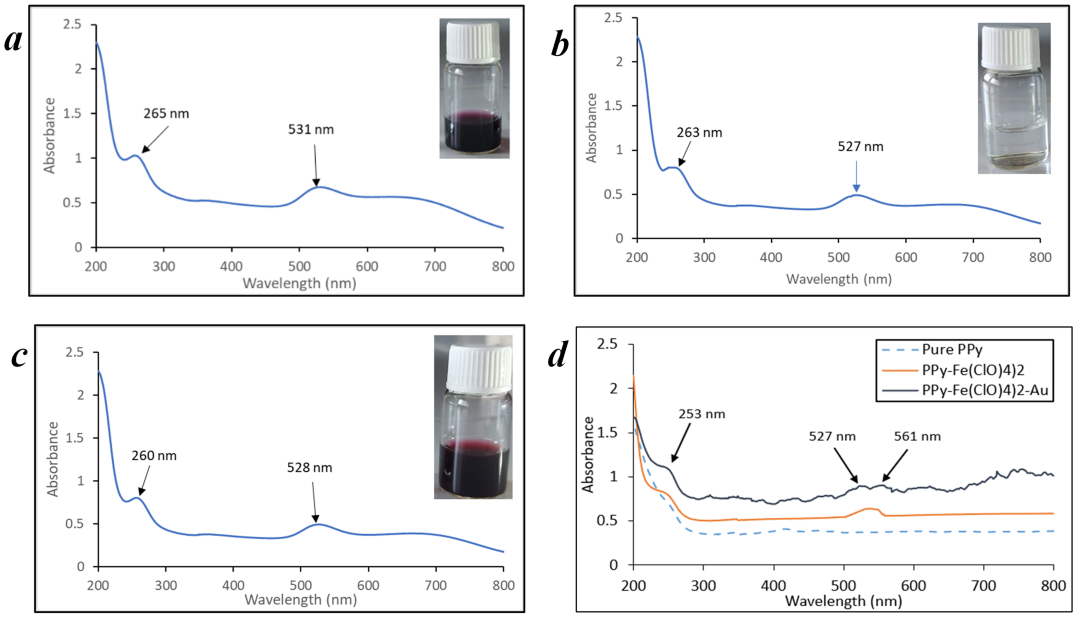

Fig 5. UV-visible spectra for Gold nanoparticle solution at different colours: a) Colourless b) pink c) Ruby red and UV-visible spectra of Pure PPy, PPy-Fe$(ClO_4)_2$ and PPy-Fe$(ClO_4)_2$-Au nanocomposite

3.5 TGA analysis:

The thermal stability of Pure PPy, PPy-Fe$(ClO_4)_2$ and PPy-Fe$(ClO_4)_2$-Au nanocomposite was determined using TGA in a nitrogen environment at a heating rate of 10 °C/min is shown in Figure 6. The onset temperature for Pure PPy, PPy-Fe$(ClO_4)_2$ and PPy-Fe$(ClO_4)_2$-Au nanocomposite as 150 °C, 160 °C and 150 °C. This is due to the improved thermal stability due to the addition of dopant and stabilizing effect of gold nanoparticles. All these samples exhibit different thermal degradation characteristics in the TGA investigation with two weight loss phases. Pure PPy displays weight loss of 14.5% and 34.6%, totaling approximately 49.1%, where the initial weight loss likely corresponds to moisture loss upto ~150 °C and the second to the decomposition of the PPy structure upto ~400 °C which is attributed to the thermal oxidative decomposition of PPy chain [25].

The decreased initial weight loss compared to pure PPy shows that the dopant $Fe(ClO_4)_2$ promotes stability in the early thermal degradation phase, most likely due to the stronger molecular interaction between PPy and $Fe(ClO_4)_2$. PPy-$Fe(ClO_4)_2$-Au nanocomposite showed two significant weight loss phases: 33.1% and 11.7%. This results in a total weight loss of roughly 44.8%, which was probably caused by moisture loss, and C, H and N decomposition which is similar to Sood et.al[9]. This implies that Au nanoparticles inhibit degradation in the second phase by serving as a heat sink, enhancing overall thermal stability. All of the samples indicate the following thermal stability trend: PPy-$Fe(ClO_4)_2$-Au > PPy-$Fe(ClO_4)_2$> Pure PPy. According to this hierarchy, $Fe(ClO_4)_2$ doping increases the thermal stability of PPy by providing molecular reinforcement and Au nanoparticles further improve this stability by maintaining structural integrity and slowing down the rate of degradation in high temperature environments. This thermal stability helps preserve sensor integrity at high temperatures, which is advantageous for applications in thermally stable gas sensors[25].

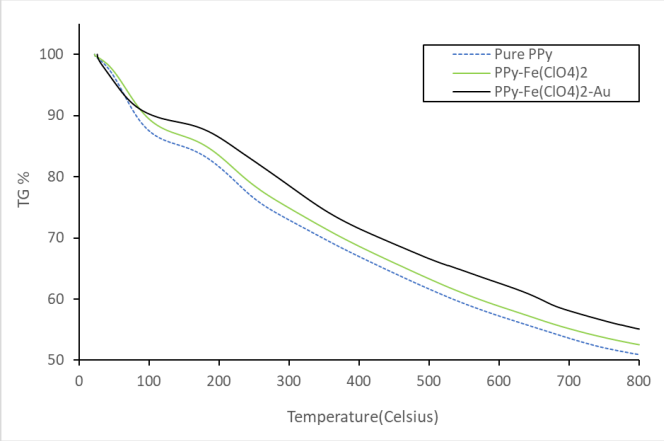

Fig 6. TGA of Pure PPy, PPy-$Fe(ClO_4)_2$ and PPy-$Fe(ClO_4)_2$-Au nanocomposite

3.6 Current-Voltage (I-V) characteristics:

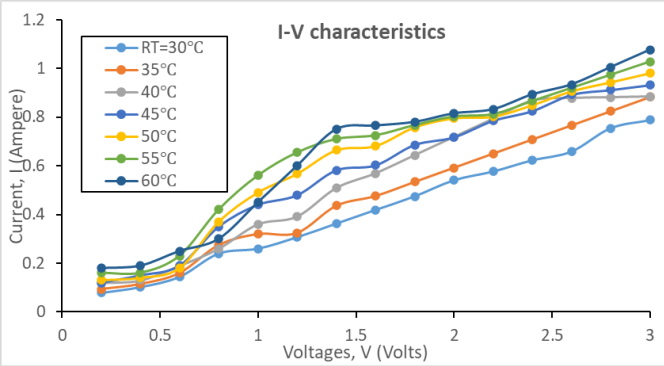

Fig 7. I-V characteristic graph of PPy-$Fe(ClO_4)_2$-Au nanocomposite at various temperatures

The nanocomposite powder is pressed under high pressure to form pellets of size 13 mm diameter. Then the I-V characteristics for all these samples were studied to evaluate electrical conductivity. The I-V characteristics for PPy-$Fe(ClO_4)_2$-Au nanocomposite are illustrated in Figure 7. It contains I-V curves at various temperature vary from Room temperature (RT =30°C) to 60°C. The curves show a consistent rise in current with voltage which clearly indicates the ohmic nature of the sample as expected according to Sood et.al[26].

Ohmic behavior is essential for sensor applications because it ensures linear and stable electrical performance, which is necessary for precise and reliable sensor operation. Rapider responses and increased sensor sensitivity are the results of this behavior, which promotes effective charge carrier mobility. The low contact resistance of Ohmic contact reduces energy loss

and electrical noise, resulting in more accurate sensor readings. Furthermore, the stability of Ohmic contacts contributes to sensor reliability and durability, making them crucial for a wide range of sensing applications[27].

The electrical conductivity calculated for all three samples using two probe method is evaluated using the formula[8],

Conductivity, $\sigma = \frac{I}{V}\frac{t}{A} = \frac{t}{R \times A}$

Where, V = voltage applied, t = Thickness of the sample, I = current, R= resistance of the sample, A = Area of the sample which is in contact with the probes.

The conductivity of PPy-$Fe(ClO_4)_2$-Au Nanocomposite is much higher as compared to Pure PPy and PPy doped $Fe(ClO_4)_2$. This may be due to the presence of Au metal on PPy matrix with addition of iron (Fe) containing dopant. The electrical conductivity of PPy-$Fe(ClO_4)_2$-Au Nanocomposite is 30.58 Scm^{-1}, is much higher than PPy samples recorded by Dave et.al.[11] which is in the order of 10^{-4} Scm^{-1}. This enhanced electrical conductivity at room temperature is crucial for the fabrication of sensors[28,29].

3.7 Gas Sensing Characteristics:

Figure 8 **a** shows the sensitivity curves for different concentrations of NH_3 gas on our fabricated gas sensor, which varies from 40 ppm to 60 ppm. The sensitivity (S) of gas sensor obtained by using the formula given by[8],

$$Sensitivity,\ S\,\% = \frac{|R_{air} - R_{gas}|}{R_{air}} \times 100\% = \frac{|\triangle R|}{R_{air}} \times 100\%$$

The Figure 8**a** shows that as the NH_3 gas concentration rises, the sensitivity of the gas sensor increases. Our main focus of research is to build this room temperature operated sensor for low ppm gases such as 40 ppm gas concentration. Thus, we plotted the Resistance versus time graph for 40 ppm gas concentration at room temperature as shown in Figure 8 **b**. To evaluate the reproducibility and repeatability of the gas sensor's performance and to comprehend the gas sensing mechanism, the NH_3 gas was passed through several times. This gives the good repeatability and recovery of sensor at low ppm of NH_3 gas as recorded by Jain et.al.[30]. During all cycles, it shows consistent behaviour during the adsorption and desorption of NH_3 gas. The response time and recovery time at this 40 ppm is 10 sec and 43 sec respectively.

The mechanism of NH_3 gas sensing by the PPy-$Fe(ClO_4)_2$-Au nanocomposite sensor involves the interaction of NH_3 with the doped PPy matrix[31]. Polypyrrole, in its doped state, contains positively charged nitrogen sites ($–N^+–$) that interact with ammonia's lone electron pair, leading to de-doping and a decrease in conductivity as NH_3 neutralizes the positive charge, forming NH_4^+. $Fe(ClO_4)_2$ enhances the conductivity and stability of the PPy matrix, while perchlorate ions (ClO_4^-) assist in maintaining the reversibility of the adsorption-desorption process. Gold nanoparticles (AuNPs) further improve sensitivity by increasing the surface area for gas interaction and facilitating efficient charge transfer. Upon removal of NH_3, desorption occurs, allowing the PPy matrix to regain its conductivity, making the mechanism reversible. This synergy between PPy, $Fe(ClO_4)_2$ and AuNPs provides high sensitivity, selectivity, and stability for NH_3 detection.

Response and recovery curves for different NH_3 gas concentrations are shown in Figure 8**c**. It demonstrates that the sensor's response time is higher at low concentrations while the recovery time rises with concentration. In order to detect NH_3 gas accurately and efficiently, a sensor should ideally have a quick recovery time in addition to a fast response time[32]. Response time of the sensor decreases with increasing concentration making it fast responsive while recovery time increases with gas concentration. Figure 8**d** shows the consistent rise in sensitivity with increasing ppm value. This shows the sensor's linearity behaviour which is significant for good sensor fabrication[33]. Figure 8**e** shows selectivity of Sensor at 40 ppm against various gases such as NH_3, NO_2, H_2S, LPG and H_2O. This shows the higher sensitivity for NH_3 gas as compared to other gases. This is highest as compared to the previous gas sensor studies by Jain et.al[30], Nguyen et.al[31] and Santos-Ceballos et.al[34]. Finally, the Figure 8 **f** depicts the long-term stability of sensor in which the graph shows sensitivity pattern of our sensor for 60 days after every 10 days. AuNPs are stable in dark and cold conditions for a longer time according to Borse et.al[17]. Our sensor shows long term stability after 60 days which makes it good sensor than the previous sensors reported by Jain et.al., This indicates the steady nature of the graph which is crucial for gas sensor. Incorporating mechanisms like UV light or thermal treatments periodically restores the sensor's active sites, maintaining performance over extended periods. The typical applications for this kind of sensor include industrial safety, indoor air quality assessment, environmental monitoring, and other applications requiring sensitive and accurate detection of gases at very low levels. Compared to sensors that need higher temperatures to function, room temperature sensors are easier to set up and utilize less energy[35] [36].

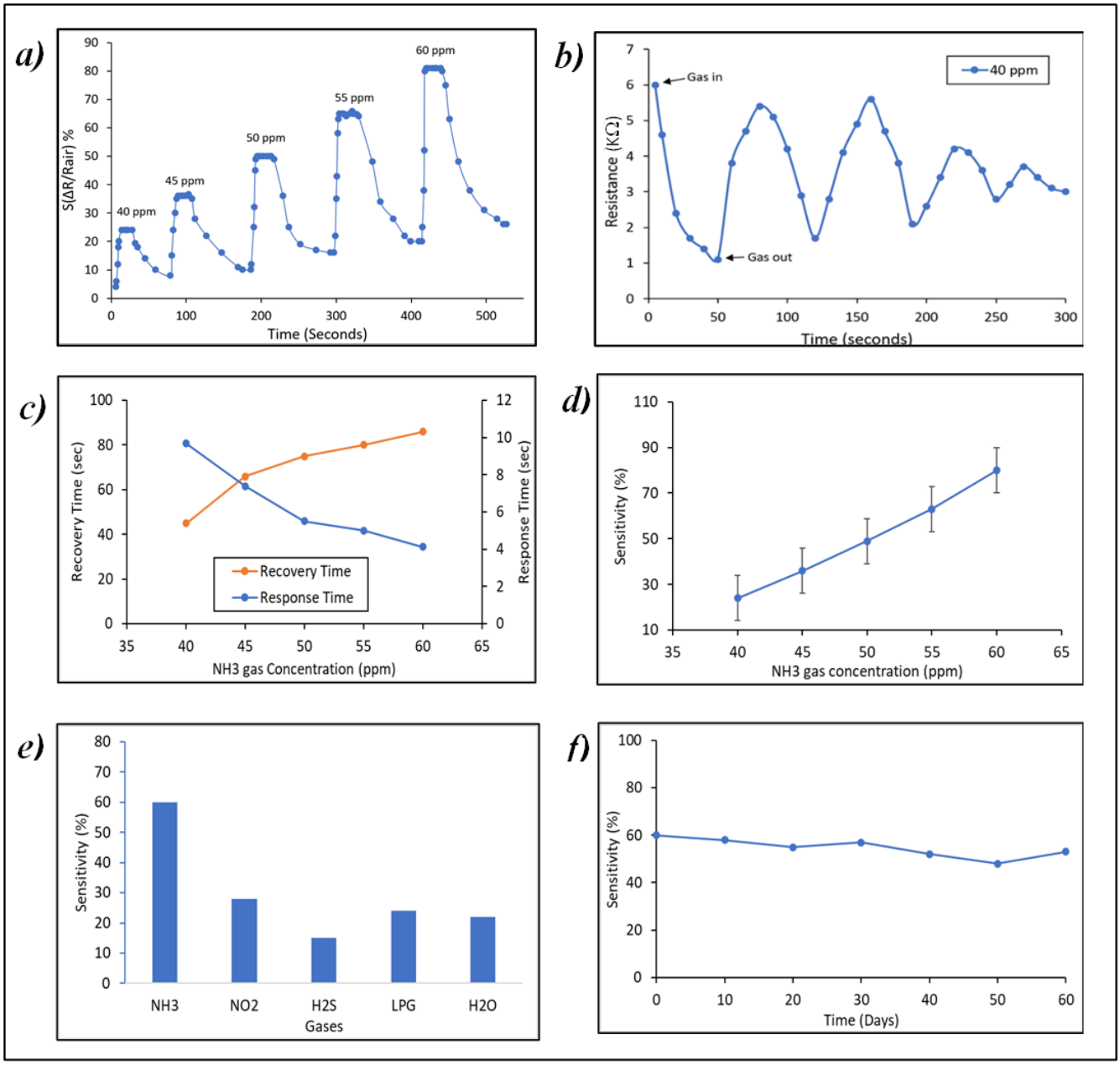

Fig 8. Gas Sensing characteristics of sensor for NH_3 gas: a) Gas sensing response at different NH_3 concentration b) Resistance vs Time relation c) Response and Recovery Time at various concentration of gas d) Sensitivity at various gas concentration (ppm) e) Selectivity study against various gases f) Long time stability study

4 Conclusion

PPy, PPy doped with $Fe(ClO_4)_2$ and PPy-$Fe(ClO_4)_2$-Au nanocomposites were successfully produced in this research to study their structural, morphological, thermal, optical, electrical, and gas sensing capabilities. According to SEM and TEM investigations, the PPy-$Fe(ClO_4)_2$-Au nanocomposite had a globular morphology with uniform distribution and better structural packing, with Au nanoparticles that were about 40 nm in size. The effective integration of $Fe(ClO_4)_2$ and Au nanoparticles was validated by FTIR and UV-visible spectroscopy, demonstrating structural interactions within the PPy matrix. The nanocomposite showed improved thermal stability according to TGA analysis, with a stability hierarchy of PPy-$Fe(ClO_4)_2$-Au > PPy-$Fe(ClO_4)_2$ > Pure PPy. The synergistic impacts of $Fe(ClO_4)_2$ and Au nanoparticles were responsible for the PPy-$Fe(ClO_4)_2$-Au nanocomposite's greatest conductivity (30.58 S/cm), according to electrical evaluation. Gas sensing studies showed that the PPy-$Fe(ClO_4)_2$-Au nanocomposite-based sensor had fast response and recovery durations (10 s and 43 s, respectively) and excellent sensitivity, reproducibility, and repeatability for NH_3 detection at low concentrations (40 ppm) at room temperature. According to these results, the PPy-$Fe(ClO_4)_2$-Au nanocomposite shows potential as a material for creating high-performance, room-temperature gas sensors that can identify NH_3 at low parts per million.

Author contribution statement

Vinod S. More: Writing – Original Draft Preparation, Conceptualization, Investigation, Minal P.Patil: Methodology. Raju P. Tandel: Data Curation, Data visualization, Experimentation. Tatyarao N. Ghorude: Supervision, Data Validation. Gitesh G. Padhye: Supervision, Methodology.

Acknowledgements

The authors gratefully acknowledge the technical support provided by the Department of Physics, N.B. Mehta Science College, BORDI, Maharashtra, India and the Sophisticated Analytical Instrument Facility (SAIF) at Indian Institute of Technology (IIT), Mumbai for support us in carrying out this work.

References

1) Kwak D, Lei Y, Maric R. Ammonia gas sensors: A comprehensive review. *Talanta*. 2019;204:713–730. Available from: https://doi.org/10.1016/j.talanta.2019.06.034.
2) Ammonia Handling Safety Guidelines and Information | Risks & Hazards. 2021. Available from: https://int-enviroguard.com/blog/how-to-protect-workers-from-ammonia-exposure/.
3) Verma A, Gupta R, Verma AS, Kumar T. Review-Recent Advances and Challenges of Conducting Polymer-Metal Nanocomposites for the Detection of Industrial Waste Gases. *ECS Journal of Solid State Science and Technology*. 2023;12(4). Available from: https://iopscience.iop.org/article/10.1149/2162-8777/acc75e.
4) Sanyal G, Jaiswal R, Chakraborty B. 2D materials-conducting polymers-based hybrids for electrochemical sensing. *2D Materials-Based Electrochemical Sensors*. 2023;2023:325–354. Available from: https://doi.org/10.1016/B978-0-443-15293-1.00012-4.
5) Kadhem SJ. Studying of Plasma- Polymerized Pyrrole at Variable Gas Flow Rates Via Plasma Jet. *Iraqi Journal of Physics*. 2021;19:44–51. Available from: https://www.researchgate.net/publication/350072024_Studying_of_Plasma-Polymerized_Pyrrole_at_Variable_Gas_Flow_Rates_Via_Plasma_Jet.
6) Kumaravel S, Kim E, Kale BB, Adhikari A, Patel R, Kundu S. Recent Developments in Conductive Polymer-Based Electro-/Photoelectrocatalytic Materials for Effective Hydrogen/Oxygen Evolution Reactions: A Review. *ChemElectroChem*. 2022;9. Available from: https://doi.org/10.1002/celc.202200724.
7) Wallace GG, Teasdale PR, Spinks GM, Kane-Maguire LAP. Conductive Electroactive Polymers- Intelligent Polymer Systems. 3rd ed. Boca Raton. CRC press. 2008. Available from: https://doi.org/https://doi.org/10.1201/9781420067156.
8) More VS, Sakhare BK, Tandel RP, Padhye GG, Ghorude TN. Electric Elegance: Enhancing Cotton Fabric with Conducting Polypyrrole for Gas Sensing Applications. *Mapana Journal of Sciences*. 2024;22:59–76. Available from: https://core.ac.uk/download/pdf/617889154.pdf.
9) Sood Y, Mudila H, Katoch A, Lokhande PE, Kumar D, Sharma A, et al. Eminence of oxidants on structural-electrical property of Polypyrrole. *Journal of Materials Science: Materials in Electronics*. 2023;34. Available from: https://link.springer.com/article/10.1007/s10854-023-10834-8.
10) Pagar SB, Ghorude TN, Nikolova MP, SenthilKannan K. Synthesis, physical, chemical, biological, mechanical and electronic studies of polypyrrole (PPy) of versatile scales for electro-mechano, pharmaceutical utilities. *Heliyon*. 2023;9(9):1–8. Available from: https://doi.org/10.1016/j.heliyon.2023.e20086.
11) Dave NV, Nerkar DM. The influence of the oxidant on structural and morphological properties of conductive polypyrrole. *Mater Today Proc*. 2021;45:5939–5943. Available from: https://www.sciencedirect.com/science/article/abs/pii/S221478532036795X.
12) Sravanthi M, Manjunatha KG. Synthesis and characterization of conducting polypyrrole with various dopants. *Mater Today Proc*. 2021;46:5964–5968. Available from: https://doi.org/10.1016/j.matpr.2020.11.762.
13) Diauudin FN, Noor SAM, Rashid JIA, Knight VF, Yunus WMZW, Ong KK, et al. Preparation and Characterisation of Polypyrrole-Iron Oxyhydroxide Nanocomposite as Sensing Material. *Advances in Materials Science and Engineering*. 2020;2020:1–11. Available from: https://onlinelibrary.wiley.com/doi/epdf/10.1155/2020/8762969.
14) Dong J, Carpinone PL, Pyrgiotakis G, Demokritou P, Moudgil BM. Synthesis of precision gold nanoparticles using Turkevich method. *KONA Powder and Particle Journal*. 2020;37:224–232. Available from: https://pmc.ncbi.nlm.nih.gov/articles/PMC7062369/pdf/nihms-1552633.pdf.
15) Lawaniya SD, Kumar S, Yu Y, Awasthi K. Nitrogen-doped carbon nano-onions/polypyrrole nanocomposite based low-cost flexible sensor for room temperature ammonia detection. *Sci Rep*. 2024;14. Available from: https://www.nature.com/articles/s41598-024-57153-4.

16) Zhao K, Shi Y, Cui M, Tang B, Zheng C, Chen Q, et al. Flexible Resistive Gas Sensor Based on Molybdenum Disulfide-Modified Polypyrrole for Trace NO2 Detection. *Polymers (Basel)*. 1940;16(13). Available from: https://www.mdpi.com/2073-4360/16/13/1940.
17) Borse V, Konwar AN. Synthesis and characterization of gold nanoparticles as a sensing tool for the lateral flow immunoassay development. *Sensors International*. 2020;1. Available from: https://www.sciencedirect.com/science/article/pii/S2666351120300516.
18) Amiri M, Golmohammadi F, Safari M, Sadeq TW. Electrochemical synthesis of polypyrrole composite with modified gold nanoparticles for electrochemical detection of ascorbic acid, dopamine and acetaminophen in different pharmaceutical samples. *Polymer Bulletin*. 2024;81:9775–9793. Available from: https://link.springer.com/article/10.1007/s00289-024-05169-1.
19) Sreevidya U, Shalini V, Bharathi KK, Kumar ES, Prakash M, Navaneethan M. Enhancing the thermoelectric performance by defect structures induced in p-type polypyrrole-polyaniline nanocomposite for room-temperature thermoelectric applications. *Journal of Materials Science: Materials in Electronics*. 2022;33:11650–11660. Available from: https://link.springer.com/article/10.1007/s10854-022-08112-0.
20) Devi R, Patel K, Sahu V, Kashyap K, Tapadia K, Maharana T. Fabrication and Characterization of Polypyrrole Nanoparticles for Supercapacitor Electrode Materials. *IOP Conference Series: Materials Science and Engineering*. 2020;798:1–7. Available from: https://iopscience.iop.org/article/10.1088/1757-899X/798/1/012034/pdf.
21) Vinila VS, Isac J, Micro and Nano Technologies. Synthesis and structural studies of superconducting perovskite GdBa2Ca3Cu4O10.5+δ nanosystems. In: and others, editor. Design, Fabrication, and Characterization of Multifunctional Nanomaterials. Elsevier. 2022;p. 319–341. Available from: https://doi.org/10.1016/B978-0-12-820558-7.00022-4.
22) Hammami I, Alabdallah NM, jomaa AA, Kamoun M. Gold nanoparticles: Synthesis properties and applications. *Journal of King Saud University - Science*. 2021;33(7):1–10. Available from: https://www.sciencedirect.com/science/article/pii/S1018364721002214?via%3Dihub.
23) Lee SH, Jung HK, Kim TC, Kim CH, Shin CH, Yoon TS, et al. Facile method for the synthesis of gold nanoparticles using an ion coater. *Applied Surface Science*. 2018;434:1001–1006. Available from: https://dx.doi.org/10.1016/j.apsusc.2017.11.008.
24) Jose D, Joseph R, John H. Synthesis, characterization, morphological and electrical studies of polypyrrole nanostructures. In: THE 3RD INTERNATIONAL CONFERENCE ON OPTOELECTRONIC AND NANO MATERIALS FOR ADVANCED TECHNOLOGY (icONMAT 2019), 3–5 January 2019, Kerala, India;vol. 2082. AIP Publishing. 2019;p. 30011–30011. Available from: https://doi.org/10.1063/1.5093829.
25) Zhang B, Xu Y, Zheng Y, Dai L, Zhang M, Yang J, et al. A Facile Synthesis of Polypyrrole/Carbon Nanotube Composites with Ultrathin, Uniform and Thickness-Tunable Polypyrrole Shells. *Nanoscale Research Letters*. 2011;6(1). Available from: https://dx.doi.org/10.1186/1556-276x-6-431.
26) Sood Y, Pawar VS, Mudila H, kumar A. Influence of Polypyrrole Morphology on Gas Sensing. *Journal of Physics: Conference Series*. 2022;2267(1). Available from: https://dx.doi.org/10.1088/1742-6596/2267/1/012050.
27) Berger C, Alquier D, Michaud JF. How to Accurately Determine the Ohmic Contact Properties on n-Type 4H-SiC. *Electronics*. 2024;13(1). Available from: https://dx.doi.org/10.3390/electronics13010217.
28) Sood Y, Singh K, Mudila H, Lokhande PE, Singh L, Kumar D, et al. Insights into properties, synthesis and emerging applications of polypyrrole-based composites, and future prospective: A review. *Heliyon*. 2024;10(13). Available from: https://dx.doi.org/10.1016/j.heliyon.2024.e33643.
29) Sood Y, Lawaniya SD, Mudila H, Katoch A, Awasthi K, Kumar A. Ultra-high performance of PPy/MoS2 2D nanocomposites for ammonia sensing. *Sensors and Actuators B: Chemical*. 2024;417. Available from: https://dx.doi.org/10.1016/j.snb.2024.136165.
30) Jain A, Nabeel AN, Bhagwat S, Kumar R, Sharma S, Kozak D, et al. Fabrication of polypyrrole gas sensor for detection of NH3 using an oxidizing agent and pyrrole combinations: Studies and characterizations. *Heliyon*. 2023;9(7). Available from: https://dx.doi.org/10.1016/j.heliyon.2023.e17611.
31) Van Nguyen K, Trung BH, Van Tuan C, Sai CD, Vu TD, Trung T, et al. Ammonia gas-sensing behavior of uniform nanostructured PPy film prepared by simple-straightforward in situ chemical vapor oxidation. *Open Physics*. 2023;21(1). Available from: https://dx.doi.org/10.1515/phys-2022-0232.
32) Zhang Z, Du H, Yi W, Sun YW, Zheng Y, Wu Y, et al. Investigation of Ammonia-sensing Mechanism on Polypyrrole Gas Sensor Based on Experimental and Theoretical Evidence. *Sensors and Materials*. 2021;33(4):1443–1454. Available from: https://pdfs.semanticscholar.org/3cad/12b2120733fa04b86eadf8b9ba53310e9060.pdf.
33) Ansari MO, Ansari SA, Cho MH, Ansari SP, Abdel-Wahab MS, Alshahrie A. Conducting Polymer Nanocomposites as Gas Sensors. *Polymers and Polymeric Composites: A Reference Series*. 2019;p. 1–30. Available from: https://link.springer.com/referenceworkentry/10.1007/978-3-319-95987-0_25.
34) Santos-Ceballos JC, Salehnia F, Romero A, Vilanova X, Llobet E. Low Cost, Flexible, Room Temperature Gas Sensor: Polypyrrole-Modified Laser-Induced Graphene for Ammonia Detection. *IEEE Sensors Journal*. 2024;24(7):9366–9374. Available from: https://ieeexplore.ieee.org/document/10453381.
35) Nikolic MV, Milovanovic V, Vasiljevic ZZ, Stamenkovic Z. Semiconductor Gas Sensors: Materials, Technology, Design, and Application. *Sensors*. 2020;20(22). Available from: https://doi.org/10.3390/s20226694.
36) Hwang JY, Lee Y, Lee GH, Lee SY, Kim HS, Kim SI, et al. Room-temperature ammonia gas sensing via Au nanoparticle-decorated TiO2 nanosheets. *Discover Nano*. 2023;18(1). Available from: https://link.springer.com/article/10.1186/s11671-023-03798-5.